



Observational signatures of proto brown dwarf formation in protostellar disks

O. V. Zakhochay¹, E. I. Vorobyov^{2,3}, and M. M. Dunham⁴

¹ Main Astronomical Observatory, National Academy of Sciences of Ukraine, Kyiv, 03680, Ukraine, e-mail: zkhohga@mail.ru

² Institute of Astrophysics, University of Vienna, Vienna, 1180, Austria

³ Research Institute of Physics, Southern Federal University, Rostov-on-Don, 344090, Russia

⁴ Department of Astronomy, Yale University, P.O. Box 208101, New Haven, CT 06520, USA

Abstract. In this work we explore the brown dwarf formation scenario via disk fragmentation. Using numerical hydrodynamic simulations, we study the gravitational fragmentation of an unstable protostellar disk formed during the collapse of a pre-stellar core with mass $1.2 M_{\odot}$. We explore the possibility of observational detection of the fragments (precursors of giant planets and brown dwarfs) in disks viewed through the outflow cavity. We show that massive and hot proto-brown dwarfs forming in protostellar disks can leave characteristic signatures at $5\text{--}10 \mu\text{m}$ in spectral energy distributions (SEDs) of young stellar objects. We demonstrate that one hour of integration time at the Atacama Larger Millimeter/sub-millimeter Array (ALMA) can be sufficient to detect the fragments in the brown dwarf mass regime.

Key words. accretion, accretion disks – brown dwarfs – hydrodynamics – instabilities – ISM: clouds – planets and satellites: formation – stars: formation – stars: low-mass

1. Introduction

According to the modern theory of stellar formation there are two distinct mechanisms of brown dwarf (BD) formation. One of them is the direct collapse of a very low mass cloud fragment whose mass straddles the substellar mass limit. The second scenario is a BD formation via the fragmentation of a massive protostellar disk. In this paper we investigate the observational properties of the protostellar disk fragmentation and study the possibility to de-

tect the first stage of BD formation. We focus on the properties of the massive fragments and explore possibilities of their direct and indirect observational detection.

2. Model description

We base our model on numerical hydrodynamics simulations of Vorobyov & Basu (2010), who studied the formation and evolution of protostellar disks subject to gravitational instability and fragmentation. The basic equations of hydrodynamics are solved on a polar grid

Send offprint requests to: O. V. Zakhochay

in the thin-disk limit. This allows us to follow the gravitational collapse of a pre-stellar condensation (core) into the star plus disk formation stage and further to the T Tauri stage when most of the parental core has accreted onto the burgeoning disk. The following physical processes are taken into account: disk self-gravity via solution of the Poisson integral and disk viscosity via α -parameterization, radiative cooling from the disk surface, stellar and background irradiation, and also viscous and shock heating. More details can be found in Vorobyov & Basu (2010). We describe the time evolution of a protostellar disk formed as a result of the gravitational collapse of a pre-stellar core with initial core mass $M_c = 1.22 M_\odot$ and ratio of rotational to gravitational energy $\beta = 8.8 \times 10^{-3}$. We have chosen this model based on our previous numerical simulations (Vorobyov & Basu 2010), which demonstrated that disks formed from pre-stellar cores with similar initial parameters undergo vigorous gravitational fragmentation in the embedded phase of star formation.

3. Hot proto-brown dwarf embryos

The number and properties of the fragments varies significantly with time. Find more details in Vorobyov et al. (2013). The majority of the fragments are characterized by $T_{\text{surf,c}} < 100$ K. However, there are fragments with midplane temperatures exceeding 10^3 K, which means that they have started evaporating dust in their interiors. This leads to a significant drop in opacity and an associated increase in the surface temperatures reaching several hundred Kelvin or even higher. In Fig. 1 we present zoomed-in images of two fragments with midplane temperature $T_{\text{mp,c}}$ exceeding 10^3 K. The black curves outline the fragments as identified by our tracking mechanism. The white circles mark the Hill radius for each fragment defined as

$$R_H = r_f \left(\frac{1}{3} \frac{M_f}{M_* + M_f} \right)^{1/3}, \quad (1)$$

where r_f is the radial distance from the protostar to the fragment and M_f is the mass of the fragment confined within the black curve.

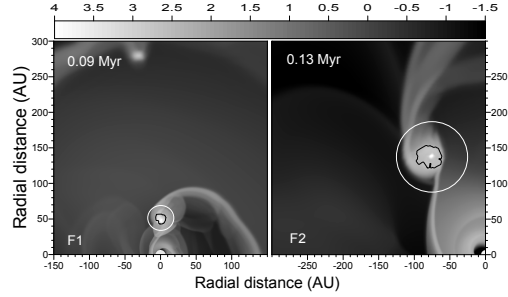


Fig. 1. Zoomed-in surface density images of two fragments characterized by midplane temperature exceeding 10^3 K. Black curves outline the fragments as found by our fragment tracking algorithm. White circles mark the corresponding Hill radii. Time elapsed since the formation of the central protostar is indicated in each panel. The scale bar is in g cm^{-2} .

The properties of these fragments are listed in Table 1. In particular, columns from left to right present: 1) the number of the fragment, 2) the time at which the fragment is seen in the disk, 3) mass of the fragment, 4) mass confined within the Hill radius M_H , 5) radial distance to the fragment, 6) radius of the fragment R_f , 7) Hill radius, 8) midplane temperature, 9) surface temperature, 10) surface density, and 11) optical depth to the midplane τ . The last four quantities were calculated at the geometrical center of the fragments. The radius of the fragment is found by calculating the surface area occupied by the fragment and assuming that the fragment has a circular form. Evidently, both fragments with $T_{\text{mp,c}} \geq 10^3$ K are in the brown dwarf mass regime.

4. Spectral energy distribution

To construct a spectral energy distribution (SED) of our model object, we split it into three constituent parts: the accreting protostar, the inner disc, and the outer dynamic disc¹. This partitioning is motivated by the specifics of our numerical model—we do not compute

¹ The outer dynamic disc may include an infalling envelope, if present. Because it is often difficult to draw a clear distinction between the disc and envelope, we refer to both simply as the outer disc.

Table 1. Characteristics of the fragments

fragment	time (Myr)	M_f (M_J)	M_H (M_J)	r_f (AU)	R_f (AU)	R_H (AU)	T_{mp} (K)	T_{surf} (K)	Σ (g cm^{-2})	τ
F1	0.09	55	68	48	8	17	1660	1020	8.7×10^4	18.5
F2	0.13	64	84	158	21	55	1375	740	3.5×10^4	32

the dynamical evolution of the system in the inner several AU (inside the sink cell) due to severe Courant limitations on the hydrodynamical time step. The SEDs calculation algorithm of our model is described in detail in Vorobyov et al. (2013). Fig. 2 presents the resulting SEDs. In particular, individual contributions from the central protostar, inner disc, and outer disc are shown by the dotted, dashed, and dash-dotted lines, respectively. The solid line is the total flux νF_ν , in units of $\text{erg cm}^{-2} \text{s}^{-1}$. The distance to our model object equals to the distance of the Perseus (250 pc) star-forming region.

A visual inspection of Fig. 2 reveals that hot and massive fragments may contribute significantly to the total radiative flux. In particular, the contribution from the outer disc has a characteristic double-peaked structure, with the peak at shorter wavelengths produced by the most massive and hot fragments in the disc. The input from the proto brown dwarf to the total flux may sometimes exceed that from the inner disc (dotted lines). As a result, the total flux may have a characteristic secondary peak at $\lambda \approx 5 \mu\text{m}$ comparable in magnitude to that produced by the protostar at $\lambda \approx 0.5 \mu\text{m}$. This feature is clearly visible when fragments have midplane temperatures exceeding 1300 K. Our method is best applied to a later evolutionary stage when most of the parental core has dissipated, thus neglecting possible photon scattering or reprocessing by the envelope. We ran simple Monte Carlo radiative transfer models of a star+disc system embedded within a core. For this purpose, we used the dust radiative transfer package RADMC (Dullemond & Dominik 2004). The SEDs of the net star+disc system shown in Fig. 2 were adopted as the

input SEDs. The results are shown in Fig. 3. Reprocessing by the dust in the core becomes significant for high inclinations but is negligible for inclinations smaller than the semi-opening angle of the outflow cavity (30 degree was assumed for the core), and the excess emission at long wavelengths from dust in the core does not hinder the ability to detect the triple-peaked SED indicative of massive disc fragments.

5. Synthetic ALMA images

In this section, we explore the possibility of detecting the fragments directly using interferometric observations with the Atacama Large Millimeter/sub-millimeter Array (ALMA). We used the SIMOBSERVE and SIMANALYZE tasks in the CASA software package² to simulate 1 hour of ALMA integration at both 230 and 345 GHz. The antenna configuration most closely corresponding to a synthesized beam of $0''.1$ (25 AU at the assumed distance of 250 pc) was selected for each frequency, since such a resolution is the minimum necessary to adequately resolve the disc into its individual fragments. With these simulated observing parameters, the 3σ detection limits of the ALMA images are approximately $0.2 \text{ mJy beam}^{-1}$ at 230 GHz and $0.8 \text{ mJy beam}^{-1}$ at 345 GHz. Figure 4 presents the gas surface densities (top row, $\log \text{g cm}^{-2}$) and simulated ALMA images at 230 GHz (middle row) and 345 GHz (bottom row), both in $\log \text{mJy beam}^{-1}$. The time elapsed since the formation of the protostar is indicated in the top row and the beam size is

² CASA, the Combined Astronomy Software Applications, is the ALMA data reduction and analysis package; see casa.nrao.edu/ for details.

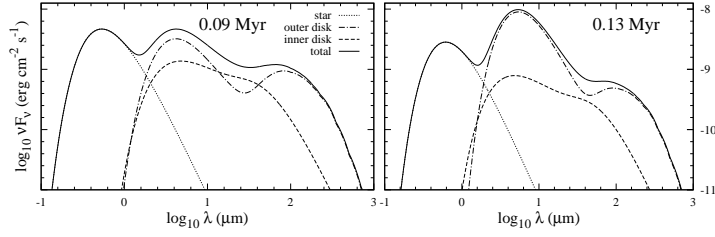


Fig. 2. Model spectral energy distributions at two times after the formation of the central star. Individual contributions from the central protostar, inner disc, and outer disc are shown by the dotted, dashed, and dash-dotted lines, respectively. The solid line is the total flux.

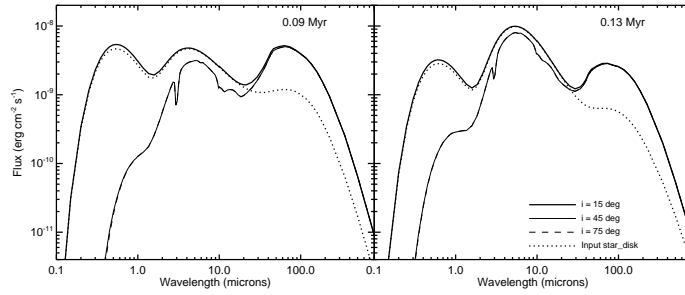


Fig. 3. Spectral energy distributions at the same two times shown in Fig. 2 obtained from Monte Carlo radiative transfer models of the net star+disk system embedded in a core (see text for details). In each panel, the model SEDs at three different inclinations are plotted, along with the star+disk SED given as an input to the models. Note that the $i = 45^\circ$ degree and $i = 75^\circ$ curves nearly merge due to an almost spherical core shape.

plotted in the right-bottom corner of each image. The black arrows in the top row point to the most massive fragments shown in Figure 1 and described in detail in Table 1. The effect of reduced resolution, images with a linear scaling and more detailed analysis are presented in Vorobyov et al. (2013).

Evidently, some of the proto brown dwarfs can be confidently detected with ALMA using just one hour of integration time. For instance, fragment F2 (0.13 Myr) at a radial distance of about 100–150 AU is clearly seen in the image and its peak fluxes are well above the detection limits of 0.2 (0.8) mJy beam⁻¹ at 230 (345) GHz. On the other hand, fragments that are located at radial distances $r \lesssim 50$ AU start to merge with the central flux peak and are more difficult to detect with our chosen resolution of 0".1. For instance, fragment F1 (0.09

Myr, at $r_f = 48$ AU) is beginning to merge with the central peak. This is not surprising considering that the corresponding linear resolution is 25 AU for the adopted distance of 250 pc. The spiral structure is clearly evident in some images.

6. Conclusions

Based on the numerical hydrodynamics simulations for the formation and evolution of a gravitationally unstable protostellar disc, we studied the observational properties of hot fragments formed via disk gravitational fragmentation. We showed that hot and massive fragments leave characteristic peaks at $\approx 5 \mu\text{m}$ in the SEDs of young protostellar discs. These features are comparable in magnitude to the flux from the central star and can potentially be used to infer the presence of a massive (\gtrsim

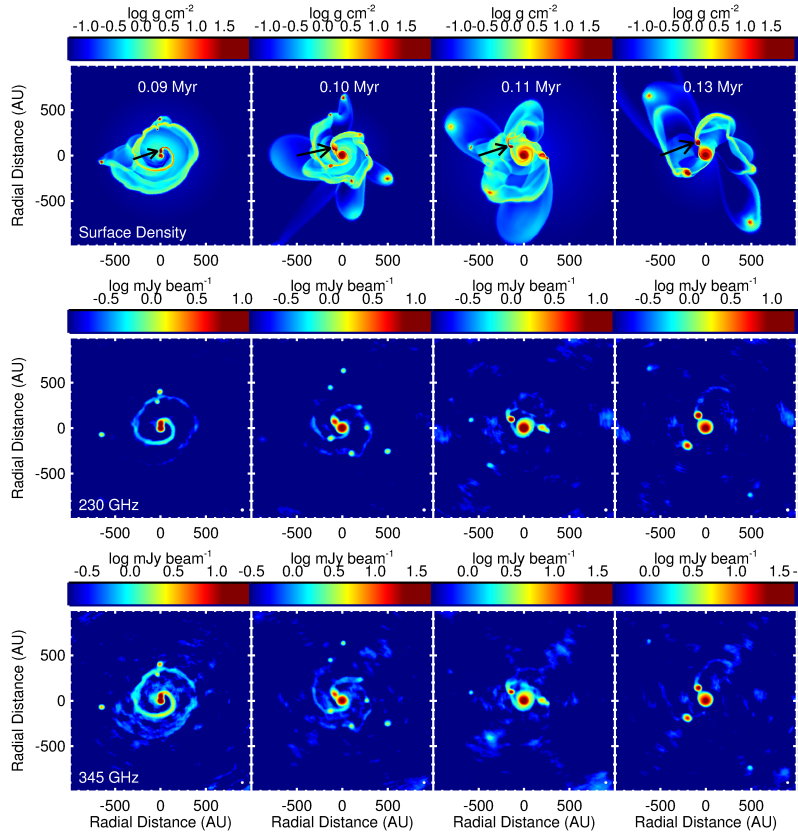


Fig. 4. *Top row:* Gas surface density maps of the inner 2000×2000 AU at four times since the formation of the central protostar. The black arrows point to the most massive fragments. *Middle and bottom rows:* The corresponding synthetic ALMA images at 230 GHz (middle) and 345 GHz (bottom). The beam size is indicated in white in the bottom right of each panel. The images are displayed on a logarithmic scaling to capture the full dynamic range of the central density peaks, surrounding fragments, and spiral disc structure.

$50 M_{\text{Jup}}$) and hot proto-brown dwarf in protostellar discs. Both fragments in our model can be detected with ALMA using just one hour of integration time and a resolution of $0''.1$, provided that the disc is favourably inclined. Using a log scaling it is possible to resolve the spiral structure and fragments at small distances $\lesssim 100$ AU.

Acknowledgements. E.I.V. acknowledges support from the RFBR grant 11-02-92601-KO. O.V.Z. acknowledges grant from the OeAD - Austrian Agency for International Cooperation in Education

& Research, financed by the Scholarship Foundation of the Republic of Austria and travel support from the LOC of the conference Brown Dwarfs come of Age.

References

- Dullemond C.P., & Dominik C. 2004, *A&A*, 417, 159
 Vorobyov E.I., & Basu S. 2010, *ApJ*, 719, 1896
 Vorobyov E.I., Zakhozhay O.V., & Dunham M.M. 2013, *MNRAS*, 433, 3256